



This is a repository copy of *Spark plasma texturing: A strategy to enhance the electro-mechanical properties of lead-free potassium sodium niobate ceramics*.

White Rose Research Online URL for this paper:
<http://eprints.whiterose.ac.uk/156685/>

Version: Accepted Version

Article:

Pinho, R., Tkach, A., Zlotnik, S. et al. (4 more authors) (2020) Spark plasma texturing: A strategy to enhance the electro-mechanical properties of lead-free potassium sodium niobate ceramics. *Applied Materials Today*, 19. 100566. ISSN 2352-9407

<https://doi.org/10.1016/j.apmt.2020.100566>

Article available under the terms of the CC-BY-NC-ND licence
(<https://creativecommons.org/licenses/by-nc-nd/4.0/>).

Reuse

This article is distributed under the terms of the Creative Commons Attribution-NonCommercial-NoDerivs (CC BY-NC-ND) licence. This licence only allows you to download this work and share it with others as long as you credit the authors, but you can't change the article in any way or use it commercially. More information and the full terms of the licence here: <https://creativecommons.org/licenses/>

Takedown

If you consider content in White Rose Research Online to be in breach of UK law, please notify us by emailing eprints@whiterose.ac.uk including the URL of the record and the reason for the withdrawal request.



eprints@whiterose.ac.uk
<https://eprints.whiterose.ac.uk/>

Spark Plasma Texturing: a strategy to enhance the electro-mechanical properties of lead-free potassium sodium niobate ceramics (KNN)

Rui Pinho¹, Oleksandr Tkach¹, Sebastian Zlotnik^{1,2}, M. Elisabete Costa¹, Jacques Noudem³, Ian M. Reaney⁴, Paula M. Vilarinho^{1*}

¹ Department of Materials and Ceramic Engineering
CICECO – Aveiro Institute of Materials
University of Aveiro
Campus Santiago, 3810-193 Aveiro, Portugal

² Lukasiwicz Research Network – Institute of Electronic Materials Technology
133 Wólczvnska Str., 01-919 Warsaw, Poland

³ CRISMAT, UMR 6508 ENSICAEN/CNRS
IUT-Caen, Université de Caen Basse-Normandie
6 Bd Maréchal Juin, 14050 Caen Cedex 04, France

⁴ Functional Materials and Devices Centre
Department of Materials Science and Engineering
University of Sheffield
Sir Robert Hadfield Building, Mappin Str., Sheffield S1 3JD, England

* corresponding author e-mail: paula.vilarinho@ua.pt

Keywords: potassium sodium niobate, spark plasma sintering, spark plasma texturing, lead free piezoelectrics

Abstract

Controlling the sintering and microstructure of lead-free potassium sodium niobate ((K_{1-x}Na_x)NbO₃, KNN) ceramics is of primary importance to optimize its piezoelectric /

ferroelectric properties. However, sintering dense and monophasic KNN remains a challenge. Here, we prepare KNN ceramics using spark plasma texturing (SPT), a modified spark plasma sintering (SPS) technique, in which uniaxial pressure is applied in an edge-free configuration, allowing ceramics to deform in the radial direction. Densification at low temperatures (1000 °C) and for short times (20 min) is achieved by SPT accompanied by constrained grain growth (average grain size = 1.4 μm), resulting in enhanced piezoelectric properties ($d_{33} = 108 \text{ pC N}^{-1}$ and $g_{33} = 21.2 \times 10^{-3} \text{ Vm N}^{-1}$). In addition, and of relevance, SPT KNN ceramics reveal a more homogeneous electrical microstructure postulated to be related with a reduced diffusion and local segregation of defects, resulting in grain cores and shells with more similar capacitances and conductivities. Our work brings new practical understanding to sintering of KNN and demonstrates the potential of alternative densification strategies for improved lead-free dielectrics.

1. Introduction

Functional oxides, which include piezoelectric ceramics, are used in a wide variety of applications, from industrial machinery to compact electronic equipment and tools. Moreover, the Internet of Things is becoming a commodity, thus increasing the need for sensors and actuators. Consequently, it is expected that the overall market for piezoelectric devices will reach \$31.33 billion by 2022 [1].

Over the last decades, $\text{Pb}(\text{Zr}_{1-x}\text{Ti}_x)\text{O}_3$ (PZT) and $\text{Pb}(\text{Mg}_{1/3}\text{Nb}_{2/3})\text{O}_3$ (PMN) have been the key piezoelectric materials due to their exceptional electromechanical properties and they dominate the market. PZT in particular is employed in numerous electromechanical devices, such as fuel injectors, motors, printing machines, piezo controlled thread guides, micro positioning systems [2] and potentially in the future, energy-harvesters for autonomous devices. However, PZT and PMN are lead-based compounds and owing to environmental concerns, relating to the toxicity of Pb and PbO [3] should be replaced with $(\text{K}_{1-x}\text{Na}_x)\text{NbO}_3$ [4], $(\text{Bi}_{0.5}\text{Na}_{0.5})\text{TiO}_3$ (BNT) and $(\text{Ba,Ca})(\text{Zr,Ti})\text{O}_3$ (BCZT), the leading PbO-free candidates [5].

Although doubts have recently been raised about its true green credentials [6], KNN remains the most promising lead-free piezoelectric system to replace PZT [4], [5], [7], [8]. The electromechanical properties are inferior to PZT but its high Curie temperature ($T_C = 420 \text{ }^\circ\text{C}$) potentially facilitates higher temperature applications and limits issues of de-poling, which are significant problems for BNT and BCZT. In

addition, the control of sintering and general ceramic engineering of KNN is far from complete, prompting opportunities for improvements in processing.

Dense KNN ceramics require relatively high sintering temperatures [9], not compatible with the high vapour pressure of alkaline elements and thus alternative processing techniques are required. Several different approaches have been attempted to decrease the sintering temperature and results reveal improved densification but usually at the expense of the electromechanical response and/or, decrease in T_C [5], [7], [8].

Apart from doping and liquid phase sintering, temperature and pressure are the most common ways to densify ceramics and control its microstructure. Several processing techniques have been developed that include pressure-assisted sintering methods, such as Hot Pressing (HP) and Hot Isostatic Pressing (HIP). In the 60's, electric current activated / assisted sintering (ECAS) was utilized for densification of high melting temperature ceramics. ECAS includes Spark Plasma Sintering (SPS) that combines the application of pressure and electric current, enabling high heating rates due to Joule heating of conductive dies [10]. Interest in SPS quickly grew and it is becoming a viable alternative to HP. The high heating rate (typically hundreds of $^{\circ}\text{C min}^{-1}$), lower sintering temperatures and shorter dwell times, controlled grain growth and stoichiometry, and the ability to fabricate nanostructured bulk materials are some of the advantages [10], [11].

Amongst the various processing methods to improve the density of KNN ceramics, HP [12]–[15] and SPS [10], [16]–[18], are the most commonly reported. Jaeger and Egerton [12] fabricated high density $(\text{K}_{0.5}\text{Na}_{0.5})\text{NbO}_3$ ceramics ($\rho = 4.46 \text{ g cm}^{-3}$) using HP (1100 $^{\circ}\text{C}$, 5600 psi for 20 min). The authors reported charge coefficient, $g_{31} = 13.1 \times 10^{-3} \text{ Vm N}^{-1}$, piezoelectric voltage coefficients, $d_{31} = 49 \text{ pC N}^{-1}$ and $d_{33} = 160 \text{ pC N}^{-1}$, electromechanical coupling coefficients, $k_{31} = 27\%$ and $k_{33} = 53\%$, and high $T_C = 420 \text{ }^{\circ}\text{C}$. Li *et al.* [18] prepared KNN ceramics by SPS at 920 $^{\circ}\text{C}$ during 5 min and studied the effect of annealing temperature and time on their properties, concluding that annealing for 4 h at 900 $^{\circ}\text{C}$ results in $\rho = 4.47 \text{ g cm}^{-3}$, $d_{33} = 148 \text{ pC N}^{-1}$, $k_p = 39.7\%$, with $T_C = 395 \text{ }^{\circ}\text{C}$. However, at an electric coercive field, $E_c = 13 \text{ kV cm}^{-1}$ a rather low remnant polarization, $P_r = 6.5 \text{ } \mu\text{C cm}^{-2}$ was obtained [18], comparing to those of $20 \text{ } \mu\text{C cm}^{-2}$ for conventionally sintered KNN ceramics [9] and of $19.4 \text{ } \mu\text{C cm}^{-2}$ for KNN single crystals [19]. Moreover, results presented in the later publication by Li

et al. present that d_{33} of their KNN ceramics prepared by SPS is just about 39 pC N^{-1} [20].

Three core variables control the SPS process: i) dc current; ii) heating rate and iii) applied pressure [10], [21]. An SPS apparatus is schematically shown in Figure 1a. It consists of a uniaxial set up, in which the punches serve as electrodes, a reaction chamber with controlled atmosphere, a direct current (dc) generator and pressure, position and temperature regulating systems. In a regular SPS cycle, the powder is introduced in a die (e.g. graphite, alumina and tungsten carbide) [10]. Both die and powder are heated by the Joule effect of the dc current, allowing temperature to rise up to $2000 \text{ }^\circ\text{C}$ with heating rates as high as $1000 \text{ }^\circ\text{C min}^{-1}$ [10]. The densification takes place in a short processing time, which limits the grain growth. Therefore, grain coarsening is limited as the heating rate increases, effectively decoupling grain growth from the densification. The application of mechanical pressure during sintering promotes the removal of pores and enhances densification [10], [21].

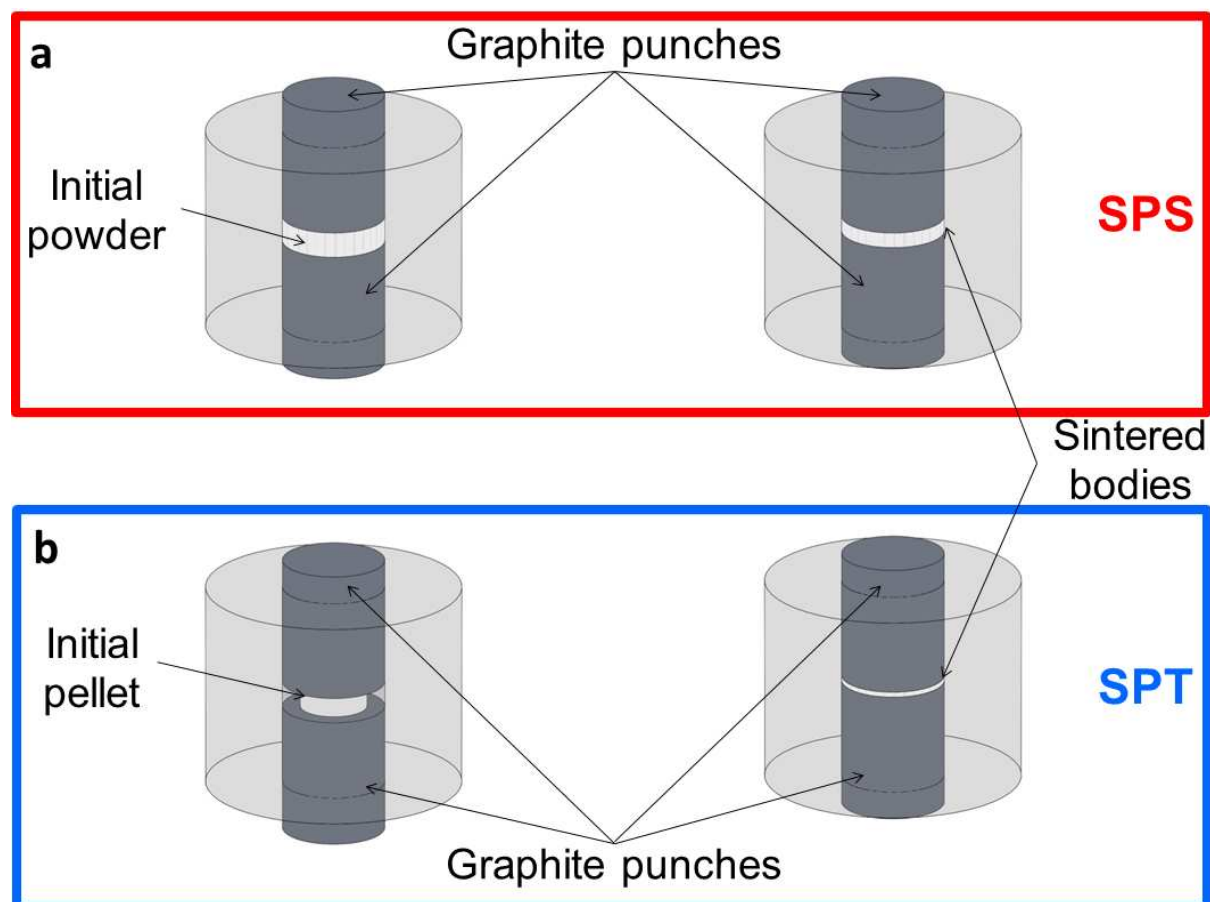


Figure 1. Schematic representation of SPS and SPT process. In SPS (a) densification is pressure assisted but in SPT (b) the sample is radial deformed during sintering cycle due to the applied pressure, resulting in 'edge-free' sintering.

One derivative method of SPS is Spark Plasma Texturing (SPT) that can be defined as an edge-free SPS and was first reported by Jacques Noudem [22]. In SPT, the sample is pre-shaped to have enough mechanical resistance to be handled. This pre-shaped sample is placed in a larger die in the SPS apparatus, resulting in edge-free sintering during the SPS cycle (Figure 1b). Noudem *et al.* [22] reported platelet shaped grains for $\text{Ca}_3\text{Co}_4\text{O}_9$ prepared by SPT with preferential orientation perpendicular to the loading direction, while conventionally sintered (CS) ceramics were characterized by round shaped grains. A remarkable improvement of density from 60% (for CS) to ~98% (for SPT) was also observed. As a result of the microstructure engineering, SPT $\text{Ca}_3\text{Co}_4\text{O}_9$ ceramics presented the lowest resistivity and the highest thermoelectric power factor (defined as σS^2 [W/mK²], where S is the Seebeck coefficient, and σ is the electrical conductivity) 30% and 800% higher than their SPS and CS counterparts, respectively [22]. The microstructure of SPT $\text{Ca}_3\text{Co}_4\text{O}_9$ ceramics is like that obtained by HP but with significantly shorter sintering times. SPT has never been used to sinter KNN ceramics.

This work addresses the sintering of undoped KNN ceramics by SPT and compares their properties with equivalent ceramics prepared by SPS. The influence of SPT on the structure, microstructure, electrical conductivity, dielectric, piezoelectric and ferroelectric properties of KNN ceramics is reported and discussed.

2. Materials and Methods

Undoped ($\text{K}_{0.5}\text{Na}_{0.5}\text{NbO}_3$) (KNN) powders were prepared by conventional solid-state reaction. Raw materials, K_2CO_3 (Merck, $\geq 99.0\%$), Na_2CO_3 (Chempur, $\geq 99.5\%$) and Nb_2O_5 (Alfa Aesar, 99.9%), were dried at 230 °C for 24 h, to eliminate adsorbents, and mixed in stoichiometric proportions, followed by ball milling with ethanol for 5 h at 180 rpm, using Teflon pots and zirconia balls. The dried powders were calcined at 900 °C for 120 min with a heating / cooling rate of 10 °C min⁻¹, to ensure the formation of a single perovskite phase (Figure S1 a)). The resultant calcined powders were ball-milled in ethanol for 5 h at 180 rpm, in Teflon pots using zirconia balls, to reduce the

particle size, resulting in a single phase KNN powder with bimodal particle size distribution of 0.2 μm and 1.8 μm (Figure S1 b)).

Ceramic pellets were prepared by SPS and SPT using a SPS furnace (model: Dr Sinter SPS 2080, Sumitomo Coal Mining Co., Ltd., Japan). For SPS, KNN powders were charged into a SPS graphite die of 20 mm diameter. After the SPS chamber was evacuated, the temperature was raised to 1000 $^{\circ}\text{C}$ at a rate of 100 $^{\circ}\text{C min}^{-1}$ and kept for 20 min, under constant pressure of 50 MPa along the z-axis (Figure 1). For SPT, differently from the SPS experiments, the powder was first pressed into a 13 mm diameter pellet and sintered at 900 $^{\circ}\text{C}$, to obtain a self-supporting sample that was placed in a 20 mm graphite die and the sintering was conducted using the same equipment and conditions as for SPS (Figure 1). After sintering, all ceramic bodies were removed from the die and annealed in air at 900 $^{\circ}\text{C}$ for 300 min.

The bulk densities of sintered bodies were measured by the Archimedes method, using water as immersion liquid. The structure of KNN powders and ceramics was evaluated, at room temperature, using X-ray powder diffraction (XRD, Malvern Panalytical X'Pert, UK, Cu- $K\alpha$ radiation) in the 20 $^{\circ}$ to 60 $^{\circ}$ 2θ range with a step length of 0.03 $^{\circ}$ and exposure time of 60 s. The residual stresses of the SPS and SPT ceramic bodies were assessed by X-ray diffraction using the Chi square method. The analysis was conducted, at room temperature, using an X-ray diffraction (X'Pert, Cu- $K\alpha$ radiation) in the 54 $^{\circ}$ and 59 $^{\circ}$ 2θ range with a step length of 0.002 $^{\circ}$ and between -70 $^{\circ}$ to 70 $^{\circ}$ ψ range with a step of 8.48 $^{\circ}$. The microstructural and local structural analysis was performed using a scanning electron microscope (SEM, Hitachi S4100, 25 keV) and transmission electron microscope (HR-TEM, Jeol 2200FS, 200 keV).

To assess the behaviour of electrical properties, the two faces of the disk-shaped ceramics were polished and platinum electrodes were painted. It is worthy to refer that a similar shape factor was ensured for all the ceramics. The electrodes were fired at 900 $^{\circ}\text{C}$, for 60 min, with heating / cooling rate of 10 $^{\circ}\text{C min}^{-1}$. Dielectric properties from room temperature to 450 $^{\circ}\text{C}$ were measured in air with a precision LCR meter (HP 4284A) under and AC voltage of 1 V in the frequency range from 0.1 to 1000 kHz. For the acquisition of the room temperature polarization and current as function of electric field, a ferroelectric tester (aixACCT TF analyzer 2000E) was used with a maximum electric field of 40 kV cm^{-1} and frequency of 60 Hz. d_{33} , was evaluated by a Berlincourt piezoelectric meter (Sinocera YE 2730A), for samples poled under 10

kV at 80 °C by Corona for 30 min. The piezoelectric voltage constant was calculated from d_{33} and the ϵ_r according with the following relationship: $g_{33} = d_{33}/(\epsilon_r \times \epsilon_0)$, where ϵ_0 is the permittivity of free space (8.85×10^{-12} F m⁻¹). Impedance data was collected from 750 to 450 °C with a step of 50 °C in air, with a precision LCR meter (HP 4284A) under AC voltage of 1 V in the frequency range of 0.35 to 1000 kHz.

3. Results

SPS and SPT sintered KNN ceramics present a dark grey coloured body attributed to the presence of oxygen vacancies ($V_{O^{\cdot}}$) formed due to the reducing atmosphere created by sintering in the graphite die [23]. Consequently, these ceramics were annealed in air at 900 °C, as described in the experimental procedure, resulting in a light cream colour, like the conventionally sintered ceramics.

All peaks in X-ray diffraction patterns of annealed KNN ceramics prepared by SPS and SPT depicted in Figure 2 correspond to a monophasic perovskite structure of monoclinic symmetry $(K_{0.5}Na_{0.5})NbO_3$ (ICPDS:00-061-0315). There are no apparent differences between these patterns, suggesting no preferential crystallographic orientation or secondary phases.

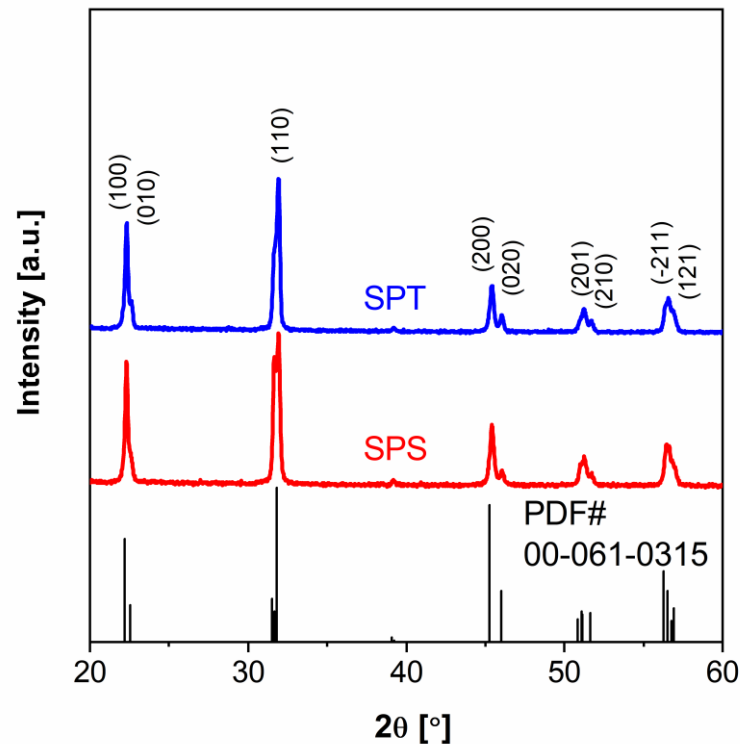


Figure 2. X-ray diffraction patterns of KNN ceramics prepared by SPS and SPT methods. The patterns may be indexed according to a monoclinic perovskite structure (PDF# 00-061-0315) with no preferred orientation.

SPT allows deformation of the grains perpendicular to the loading axis [24]. It is expected therefore, that the distribution and levels of stress of these ceramics are different from other sintering methods. As recently reported, stresses applied during sintering trigger the nucleation and growth of faults in the lattice of BaLa₄Ti₄O₁₅ ceramics, revealing a strong correlation between the high concentration of structural defects and the development of anisotropic microstructures, which tune the properties of these ceramics [25]. Hence, residual stresses in SPS and SPT KNN ceramics were evaluated by the Chi square method.

Evaluation of stresses was performed from the (-211) peak shift as a function of tilt angle (Ψ). As shown in Figure 3, both SPS and SPT KNN data could be linearly fitted, while the fitting line presents a negative slope which is an indication of a compressive stress state in both ceramics. SPT ceramics reveal a higher gradient linear fit compared with SPS. From the slope of the linear fit one may calculate the residual stresses according to:

$$\varepsilon_{\phi,\psi} = \frac{d_{\psi} - d_n}{d_n} = \frac{(1 + \nu)}{E_Y} \sigma_{\phi} \sin^2 \Psi \quad \text{Equation 1}$$

where $\varepsilon_{\phi,\psi}$ is the elastic lattice strain in a direction defined by the Euler angles Φ and Ψ with respect to the specimen normal, d_{ψ} is the lattice spacing of {hkl} planes in the direction defined by Ψ , d_n is the corresponding strain-free lattice spacing defined by $\Psi = 0^\circ$, E_Y is the modulus of elasticity, ν is the Poisson ratio and σ_{ϕ} is the residual macroscopic stress [26]. Then assuming $E_Y = 104$ GPa and $\nu = 0.27$ [27], stress values of 32 ± 46 MPa and 108 ± 48 MPa, can be obtained for KNN ceramics prepared by SPS and SPT, respectively, rearranging Eq. 1 as:

$$\sigma = \frac{E_Y}{1 + \nu} m \quad \text{Equation 2}$$

where m is the slope of the linear fit of the normalized lattice spacing as function of $\sin^2\psi$.

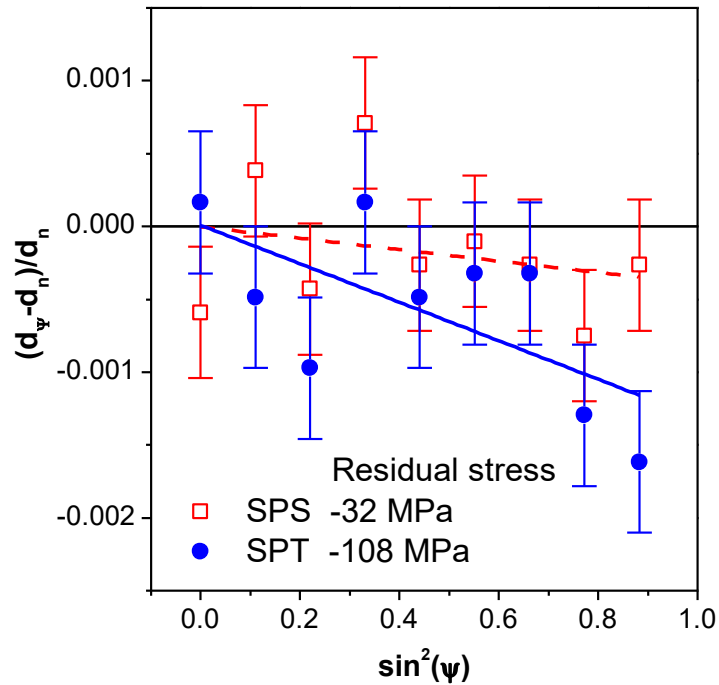


Figure 3. Lattice spacing of KNN ceramics prepared by SPS (open squares) and SPT (solid circles), as a function of $\sin^2(\psi)$. The negative slope of the linear fit (solid line for SPT and dash line for SPS) is an indication of compressive residual stress in both ceramics. The calculated residual stress is 32 and 108 MPa for SPS and SPT KNN, respectively.

The relative densities (considering KNN theoretical density of 4.51 g cm^{-3} [12]) of SPS and SPT KNN are 96.0% and 99.8%, respectively. Whereas the SPS conditions appear to be not the best to get high density of KNN ceramics, the same conditions used for SPT resulted in ceramics with one of the highest relative density reported for undoped KNN (Table 1).

Table 1. The dielectric, piezoelectric and ferroelectric properties of SPS and SPT KNN ceramics in comparison with equivalent reported physical properties of KNN single crystals and KNN ceramics prepared by CS, SPS and HP.

KNN type	Relative densification [%]	Average grain size [μm]	ϵ_r	ϵ_r at T_C	T_{O-T} [$^{\circ}\text{C}$]	T_C [$^{\circ}\text{C}$]	d_{33} [pC N^{-1}]	g_{33} [$\times 10^{-3} \text{ Vm N}^{-1}$]	P_r [$\mu\text{C cm}^{-2}$]	E_c [kV cm^{-1}]
SPS ceramics	96	3.0	736	4160	207	386	95	14.6	17.2	18.0
SPT ceramics	99.8	1.4	576	4672	204	370	108	21.2	19.7	11.9
Single crystal [19]			300		215	429	160	60.3	19.4	10.6
CS ceramics [9]	95.3		472		~ 190	~ 400	110	26.3	20.0	20.0
SPS ceramics [18] ([20])	99		606			395	148 (39)	27.6	6.5	13.0
HP ceramics [12]	98.9		420				160	43		

All ceramics present a microstructure with low porosity (Figure 4, corroborating the measured density), are homogeneous and characterized by cuboid grains, typical for KNN. The average grain size of ceramics prepared by SPT (1.4 μm) is approximately 50% smaller than SPS (3.0 μm) with the narrowest particle size distribution (range distribution for SPT and SPS are [1:3] and [1:7] μm , respectively).

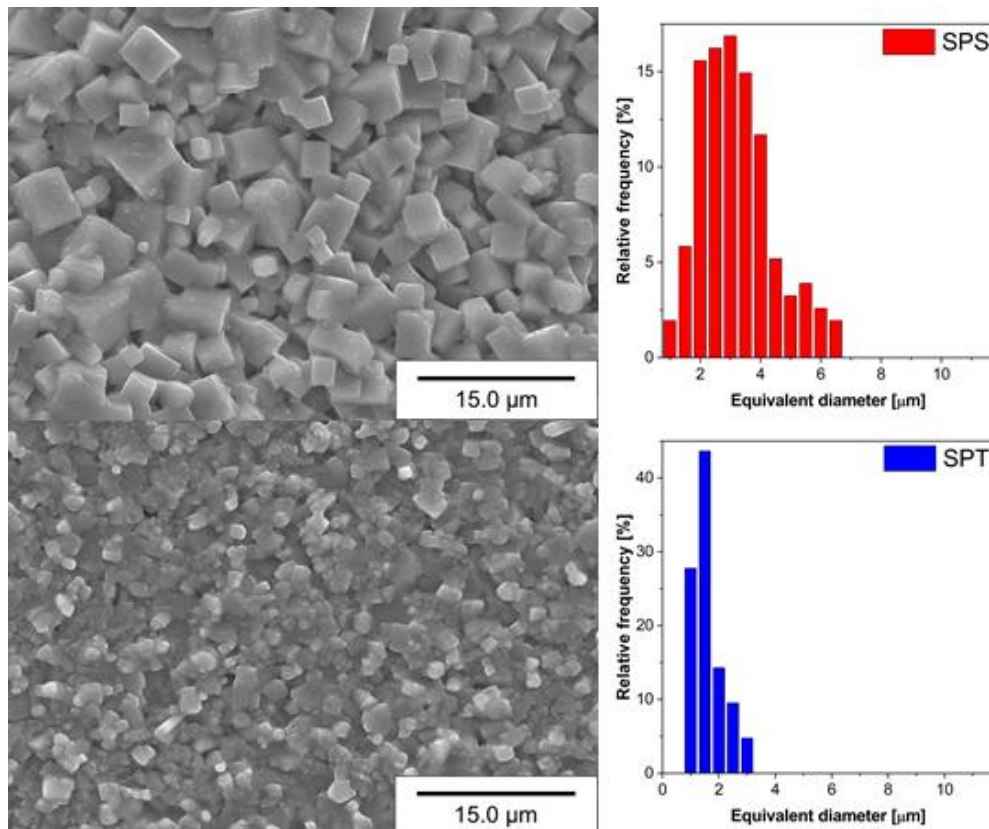


Figure 4. SEM micrographs (left) and grain size distribution (right) of KNN ceramics prepared by SPS (top) and SPT (bottom). The grains are cubic-like shaped with an average grain size of 3.0 μm and 1.4 μm for SPS and SPT, respectively.

Transmission electron microscopy (TEM) of SPS and SPT KNN ceramics (Figure 5) identified the presence of a tetragonal tungsten bronze (TTB) phase. The electron diffraction patterns acquired along the [001] direction, show the characteristic cross-like intensity distribution related to the b-glide plane in the P4/mbm space group of potassium niobate ($\text{K}_{5.75}\text{Nb}_{10.85}\text{O}_{30}$). This phase was not detected by X-ray diffraction (Figure 2) and the amount of TTB grains is scarce within both specimens. The origin of this phase on KNN ceramics can be attributed to the volatilization of alkali

species at high temperatures (the vapour pressures at 1145 °C of Na₂O and K₂O are 5.6 and 69 Pa, respectively) [28].

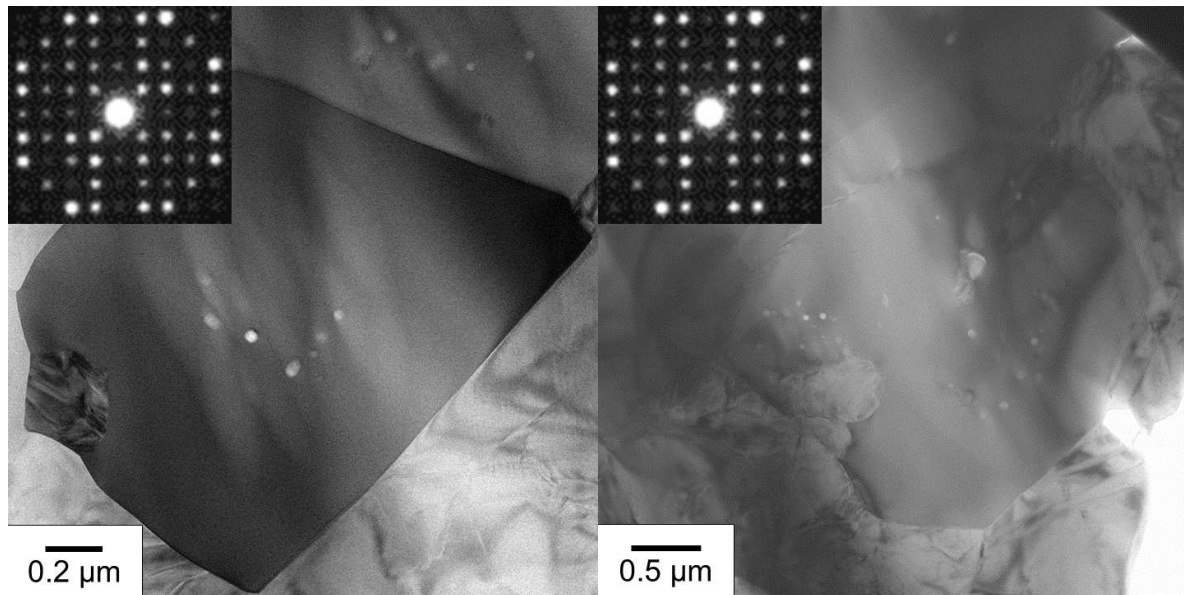


Figure 5. TEM micrographs, collected across the [001] zone axis of KNN prepared by SPS (left) and SPT (right). The presence of the tetragonal tungsten bronze grains is found and confirmed by the electron diffraction patterns, which show a characteristic cross of weak intensities related to b-glide in P4/mbm symmetry.

Figure 6a depicts the relative permittivity (ϵ_r) dependence on the temperature, measured on heating at a frequency of 1 kHz for SPS and SPT KNN. Each curve exhibits two frequency independent peaks corresponding to the tetragonal-cubic phase transition ($T_C = 386$ and 370 °C, respectively) and orthorhombic / monoclinic to the tetragonal phase transition ($T_{O-T} = 207$ and 204 °C, respectively). Compared to KNN single crystals grown by a high temperature self-flux method ($T_{O-T} = 215$ °C, $T_C = 429$ °C) [19], all ceramics exhibit lower phase transition temperatures (Table 1). However, in comparison to T_C of 395 °C reported for SPS KNN ceramics by Li *et al.* [18] and shown also in Table 1, the temperature difference is not so large. Moreover, the permittivity values reported here and in Ref. 18 are rather close as well. At room temperature, SPS and SPT KNN exhibit ϵ_r values of 736 ($\epsilon_r = 4160$ at T_C) and 576 ($\epsilon_r = 4672$ at T_C), respectively (Table 1). The room temperature ϵ_r for SPS KNN ceramics reported by Li *et al.* [18] was found to be 606, while that for KNN single crystals is 300 [19], which is lower than that for SPS and SPT KNN ceramics. T_C of 416 °C and room

temperature ϵ_r of 550 were reported as well for KNN ceramics prepared by SPS under 60 MPa at 1040 - 1100 °C for 3 min by Wang *et al.* [29].

The dissipation factor $\tan\delta$ for our SPS KNN is also rather high reaching 0.377 at room temperature, whereas between 100 and 200 °C it lowers to around 0.063, as shown in Figure 6b. The value of $\tan\delta$ for SPT KNN is just 0.045 at room temperature, dropping to 0.021 around 100 °C, although with further heating above 250 °C $\tan\delta$ reveals non-monotonous increase, surpassing the values for SPS KNN above 370 °C. Li *et al.* reported the room temperature $\tan\delta$ of 0.036 for their SPS KNN ceramics [18], while that observed by Wang *et al.* was about 0.045 [29].

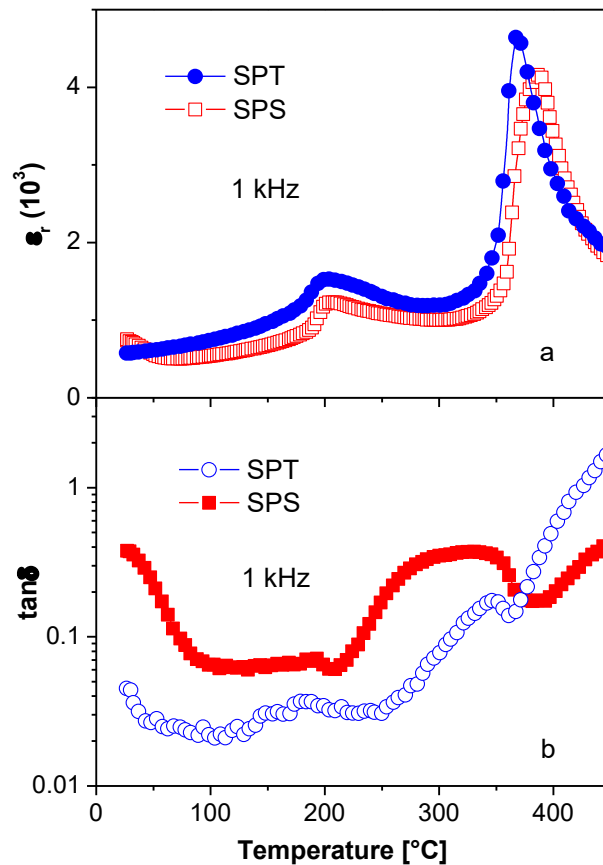


Figure 6. Temperature dependence of the relative permittivity ϵ_r (a) and dissipation factor $\tan\delta$ (b) for SPS (squares) and SPT (circles) undoped KNN ceramics at 1 kHz. Two phase transitions, corresponding to monoclinic-tetragonal and tetragonal-cubic phases, are present in all the ceramics but slightly shifted to lower T_C for SPT in comparison with SPS KNN.

The comparison of the polarization versus electric field (P - E) and current versus electric field (I - E) curves of SPS and SPT KNN at room temperature are shown in Figure 7. As seen from Figure 7a, SPS and SPT KNN exhibit well-saturated P - E curves with a typical square-like shape and remnant polarization, P_r , of $17.2 \mu\text{C cm}^{-2}$ and $19.7 \mu\text{C cm}^{-2}$, respectively, as also listed in Table 1. P_r for SPS KNN is high in regard to $15.3 \mu\text{C cm}^{-2}$ and particularly to $6.5 \mu\text{C cm}^{-2}$ observed for the corresponding ceramics by Wang *et al.* [29] and Li *et al.* [18], respectively. Comparing with $P_r = 19.4 \mu\text{C cm}^{-2}$ for KNN single crystals [19] the remnant polarization is slightly lower in the case of SPS KNN but is very close in the case of SPT KNN ceramics in agreement to their almost 100% density. Moreover, the coercive field of SPS KNN is 18 kV cm^{-1} , being rather similar to that of 20 kV cm^{-1} reported for conventionally sintered KNN ceramics [9], whereas for SPT KNN, E_c is 11.9 kV cm^{-1} , being close again to that of 10.6 kV cm^{-1} , observed for KNN single crystals [19]. Li *et al.* and Wang *et al.* reported also room temperature E_c values of 13 kV cm^{-1} and 10.2 kV cm^{-1} , respectively, for their SPS KNN ceramics [18,29].

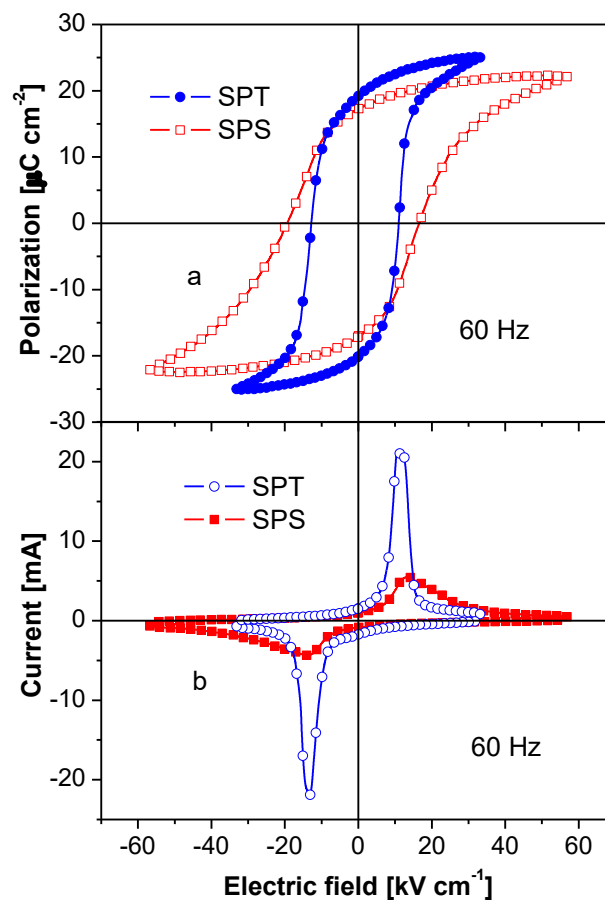


Figure 7. Polarisation versus electric field P - E hysteresis (a) and current versus electric field I - E loops of the undoped KNN ceramics prepared by SPS (squares) and SPT (circles). Well saturated P - E loop for SPT KNN with characteristic double peak I - E curve indicates well defined ferroelectric domain switching.

The characteristic maxima of the current curves, related to the switching of the ferroelectric domains, are clearly observed for SPS and SPT KNN in Figure 7b. The broad peak of the SPS KNN I - E loop may indicate contributions to conductivity from V_O'' , as discussed later. The P - E loop of SPT KNN denotes improved ferroelectric properties with a well-saturated curve. Moreover, the coercive field is lower than the SPS counterpart, which suggests a lower or different defect concentration / type [30]. The I - E curve of SPT KNN exhibits a sharp peak, which points to well-defined ferroelectric domain switching.

The piezoelectric coefficient (d_{33}) as well as the piezoelectric constant (g_{33}) values for KNN ceramics prepared by SPS and SPT are 95 and 108 pC N⁻¹ as well as 14.6×10^{-3} and 21.2×10^{-3} Vm N⁻¹, respectively, as also indicated in Table 1. The d_{33} of SPT KNN is intermediate between polycrystalline (~ 80 pC N⁻¹) and single crystal undoped KNN (80 – 160 pC N⁻¹) [19]. The d_{33} of SPS KNN is lower due to a higher / different defect concentration / type in these ceramics (probably V_O'') in agreement with the P - E and I - E loops.

Figure 8 shows the Nyquist plots of KNN sintered by SPS and SPT. The impedance values were normalized, being multiplied by the geometric factor A/h , where A is the electrode area and h is the sample thickness. The data displayed as arcs, which intercept the Z' axis shows that extrapolated overall resistivity of the SPT ceramics is lower than that of SPS ones. The observed arcs indicate also the possibility of using an electrical circuit model based on a resistor (R) parallel to a capacitor (C) to describe the ac electrical response of KNN ceramics. Generally, a single semi-circular arc in Nyquist plot can be modelled by a single R parallel to C (R//C) module, which represents the contribution of a single electroactive region of the ceramic, i.e. the grain bulk, the grain boundary, a secondary phase, etc. When two semi-circular arcs are present, one of them corresponding to lower frequencies may be attributed to the bulk response, while another arc at higher frequencies can be due to the grain boundary response [31].

Although only single arcs are seen in Figure 8, their shape is not close enough to that of semicircle, indicating that there is a possibility of two contributions with similar parameters. The information on the contributions of the various regions of the ceramics can be assessed when comparing the frequency spectra of both the impedance and modulus imaginary parts, i.e. the frequency dependence of Z'' and M'' , respectively. The complex modulus (M^*) is related to the complex impedance (Z^*) by the following relation:

$$M^* = j\omega C_0 Z^* \quad \text{Equation 3}$$

where ω is the angular frequency ($\omega=2\pi f$) and C_0 is the capacitance of the empty cell.

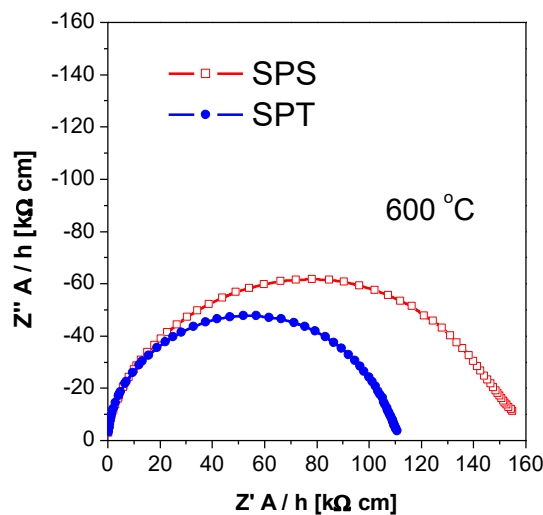


Figure 8. Nyquist plot for undoped KNN ceramics prepared by SPS (open squares) and SPT (solid circles) and measured at 600 °C within the frequency range 0.35 to 1000 kHz.

The spectra of normalized Z'' and M'' of SPS and SPT KNN ceramics are presented in Figure 9 for a temperature of 600 °C. For both SPT KNN and SPS KNN ceramics a gap exists between the frequencies corresponding to Z''_{max} and to M''_{max} thus suggesting that a series of two R//C modules ($R_1//C_1$ and $R_2//C_2$) will be required to properly describe the ac response of each of these ceramics. It is noted, however,

that for SPS KNN the mismatch between the Z''_{max} and to M''_{max} frequencies is much larger than that for SPT KNN.

Then, the values of R and C may be determined from Z''_{max} and M''_{max} using the followings equations:

$$R = 2 \times Z''_{max} \quad \text{Equation 4}$$

$$C = \frac{C_0}{2M''_{max}} \quad \text{Equation 5}$$

Thus, Eqs. 4 and 5 provide the calculation of the largest resistance and of the smallest capacitance. The remaining components, *i.e.* the smaller resistance and the larger capacitance, may be determined from the time constant τ ($\tau = RC$), being $\tau = 1/(2\pi f_{max})$.

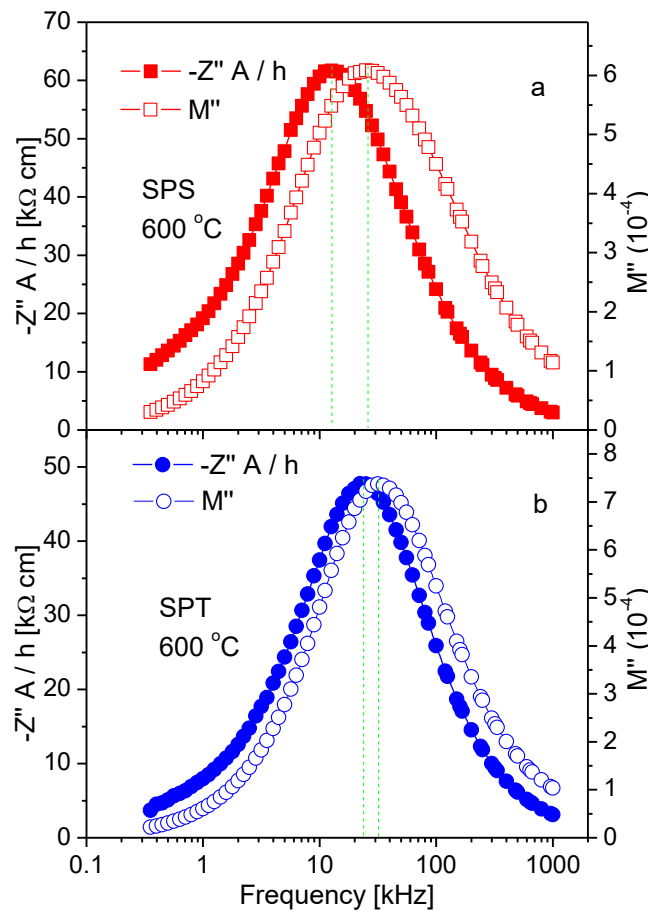


Figure 9. Normalized Z'' (solid symbols) and M'' (open symbols) of undoped KNN ceramics prepared by SPS (a) and SPT (b), measured as function of frequency at 600 °C.

Using the values of C_1 , C_2 and R_1 , R_2 calculated for SPS and SPT KNN ceramics, their temperature variations between 450 and 750 °C are presented as a Curie-Weiss plot in Figure 10a and Arrhenius plot in Figure 10b, respectively. The magnitude of the capacitances is in the order of 10^{-9} to 10^{-10} (F), consistent with bulk ferroelectric ceramics [32]. Moreover, the capacitance data follow well the Curie-Weiss law $1/C \sim T - T_C$, with Curie temperature T_C around 400 °C, as shown in Table 2, related to the paraelectric to ferroelectric phase transition of KNN. In electroceramics with different electroactive regions, the lowest capacitance is often attributed to the bulk response, while the largest R value is related to grain boundaries. However, the grain boundary capacitance is not expected to follow the Curie-Weiss law [32]. Therefore, the two contributions distinguished for SPS and SPT KNN should not be related to the bulk and grain boundaries but rather to the grain core and grain shell, perhaps slightly differing in composition that affects the Curie temperature. The higher temperature T_{C1} should be related to the grain core, while the lower one T_{C2} has to be associated with the grain shell. Such composition inhomogeneity is very probable in ceramics with volatile alkali elements (as is the case of KNN), although it seems to be lower in the case of SPT ceramics, resulting in closer T_{C1} and T_{C2} values, comparing to the SPS case.

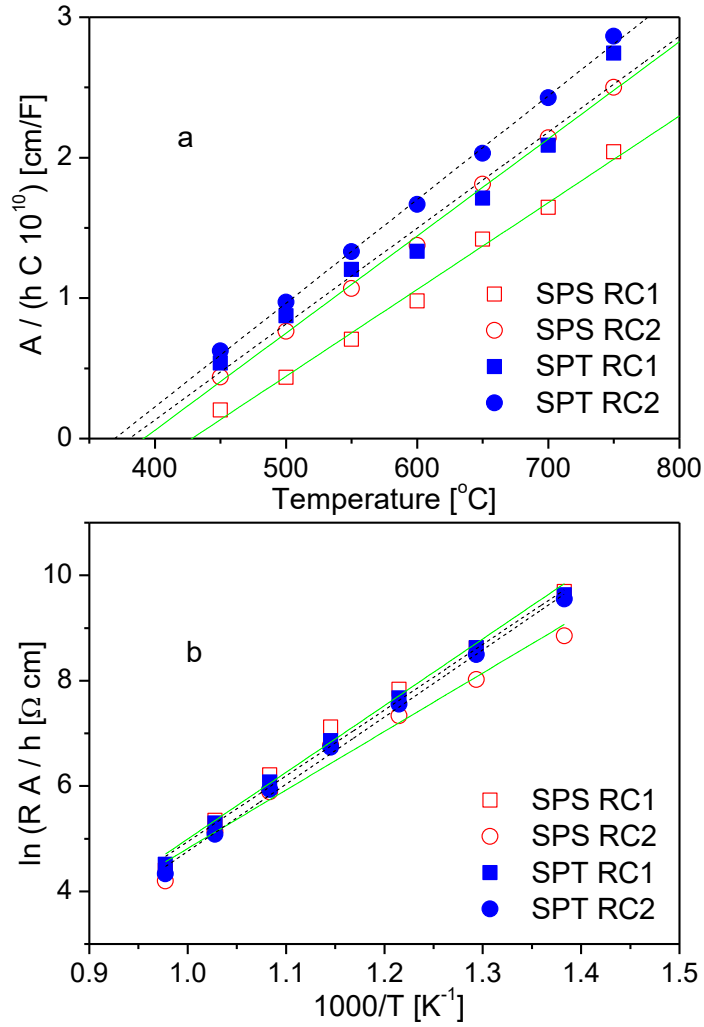


Figure 10. Plots of the normalised inverse capacitances versus temperature (a) and \ln of normalised resistances versus inverse absolute temperature (b) calculated from the impedance and electric modulus spectra for undoped KNN ceramics prepared by SPS (open symbols) and SPT (solid symbols). Linear fits (solid lines for SPS and dash lines for SPT KNN) indicate that all the capacitances follow the Curie-Weiss law, while all the resistances follow the Arrhenius law.

The resistances increase with decrease in temperature. To identify the conduction mechanisms, activation energy (E_a) for conduction ($\sigma = 1/R$) was calculated assuming the Arrhenius behaviour:

$$\sigma = \sigma_0 \exp\left(-\frac{E_a}{k_B T}\right) \quad \text{Equation 6}$$

where σ_0 is a pre-exponential factor, k_B is the Boltzmann constant and T is the absolute temperature. Then the activation energy E_a is deduced from the slope n based on the following expressions:

$$\ln(\sigma) = \ln(\sigma_0) - \frac{E_a}{k_B T} \quad \text{Equation 7}$$

$$E_a = -k_B \times n \quad \text{Equation 8}$$

as summarized in Table 2. Values of E_a ranged from 0.96 to 1.10 eV and are associated with charge transport by $V_O^{\bullet\bullet}$ [33]. Once again, E_{a1} and E_{a2} values, corresponding to the grain core and shell conductivity, respectively, are closer in the case of SPT ceramics, comparing to SPS ones, in agreement with a reduced composition inhomogeneity in SPT KNN ceramics.

Table 2. Curie temperature (T_C) and activation energy (E_a) for conductivity values deduced from IS data for KNN ceramics prepared by SPS and SPT. T_{C1} is the Curie temperature associated to the grain core, while T_{C2} is associated with the grain shell. Similarly, E_{a1} and E_{a2} values, correspond to the activation energy of grain core and shell conductivity.

KNN ceramics	T_{C1} [°C]	T_{C2} [°C]	E_{a1} [eV]	E_{a2} [eV]
SPS	428±7	391±5	1.09±0.05	0.96±0.06
SPT	381±20	369±5	1.07±0.02	1.10±0.03

The results presented above are summarized in Table 1 and demonstrate that SPT KNN ceramics exhibit the highest density, smallest grain size with the narrowest size distribution, highest residual stress, high d_{33} and low coercive field in comparison with SPS KNN. In addition, the transition temperatures of SPS and SPT KNN are shifted to lower temperatures, when compared with single crystal KNN. Notably, a more homogeneous chemical microstructure and thereby electrical behaviour (closer Curie temperatures and activation energies for the grain cores and shells) was observed for SPT KNN in comparison to SPS KNN.

3. Discussion

The application of external pressure to a powder compact results in direct increase of the densification driving force, as well as densification kinetics. As the densification rate is enhanced, the sintering temperature and sintering time can be reduced and grain growth suppressed, due to particle rearrangement and agglomerate destruction [11], [34]. As a result, SPS and SPT KNN ceramics reach a higher density at lower temperature and sintering times, compared with the CS KNN ceramics [9]. Moreover, SPT KNN ceramics sintered at 1000 °C for 20 min reveal almost 100% density (Table 1). Additionally, grain growth is suppressed for pressure assisted sintering (SPS and SPT) compared with CS [9]. SPT KNN presents the smallest average grain size with the narrowest grain size distribution (Figure 4).

In this work, both SPT and SPS ceramics were heated due to the Joule effect that results from current flow in the graphite die. When the appropriate sintering temperature is reached, pressure is applied, and samples are deformed, as shown in Figure 1. Since the only difference between the SPS and SPT resides in the edge-free nature of the sintering method of SPT, we speculate that the deformation of the material without constraints is critical in explaining the different microstructure / properties.

The absence of lateral constraint in SPT allows the ceramic to deform in the radial direction and the radial diameter increases. During the deformation, the particles slide, resulting in: i) neck destruction; ii) particle rearrangement, and iii) destruction of agglomerates. Consequently, improved density and reduced grain coarsening are expected [35] and observed in SPT KNN.

In SPS due to die constraint, KNN does not undergo radial deformation and associated rearrangement. SPS KNN reaches high densities due to the applied pressure but grain growth is not markedly impeded, resulting in a higher average grain size (Figure 4).

The differences in microstructure described above are reflected in the dielectric and piezoelectric response. The highest ϵ_r at T_C is observed for SPT KNN, $\epsilon_r = 4762$. Moreover, the P - E loop for SPT KNN is square shaped, characteristic of a low loss ferroelectric, as demonstrated by the two peaks in the I - E curves, and by the low coercive field, $E_C = 11.9 \text{ kV cm}^{-1}$. Such coercive field is close to that for KNN single crystals and much lower than that for CS KNN ceramics [9]. (*P_r* of SPT

KNN ($19.7 \mu\text{C cm}^{-2}$) is comparable to those of KNN single crystals and CS KNN ceramics. The high density of SPT KNN together with an easy ferroelectric domain switching accounts for the high piezoelectric coefficient, $d_{33} = 108 \text{ pC N}^{-1}$.

In addition, we also advocate that during dynamic deformation of the KNN particles in SPT, diffusion and point defect creation / distribution is markedly affected. Under these conditions, diffusion to the grain boundaries and local segregation of defects is reduced and the final distribution of defects is more homogeneous, resulting in grain core and shell with more similar behaviour for capacitances and conductivities (see Figure 10). We hypothesize that this unusual observation along with small grain size and the absence of pores, electrical homogeneity is critical in increasing the electric breakdown strength of a given ceramic (E_{BDS}).

In comparison, the lower density of SPS KNN ceramics and the larger average grain size and broad grain size distribution may explain the differences in electrical behaviour of SPS KNN. Both SPS and SPT ceramics were annealed in air at $900 \text{ }^\circ\text{C}$ for 300 min to re-oxidize the ceramics sintered in the graphite die. Although the annealed ceramics exhibit a whitish colour, indicative of an almost complete oxidation, and since the oxidation in ceramics occurs mainly via the grain boundaries (fast diffusion pathways), it is plausible that re-oxidation requires significantly more lattice diffusion (slower) than for samples with a smaller average grain size. The presence of a higher residual concentration of $V_{\text{O}}^{\bullet\bullet}$ in SPS KNN ceramics may certainly explain the 'lossy' P - E behaviour, the broad peaks in the I - E loop and the lower d_{33} (95 pC N^{-1}). $V_{\text{O}}^{\bullet\bullet}$ clamp ferroelectric domains [30] through the formation of defect dipoles. The clamped ferroelectric domains are harder to switch, resulting in higher coercive field, $E_c = 22 \text{ kV cm}^{-1}$, less domain switching and therefore reduced d_{33} , as observed.

The residual compressive stress in SPT KNN ceramics is 108 MPa, triple that for SPS KNN ceramics (32 MPa). A material will not exhibit ferroelectric behaviour if the structure is centrosymmetric but significant off-centring of the B ions favours a larger intrinsic piezoelectric effect and spontaneous polarisation. The larger compressive stress for SPT KNN ceramics may facilitate off-centring and enhance the piezoelectric and ferroelectric response. Kim *et al.* [36] defined a weighted off-centre coefficient (d_w) and verified for $(1-x)(\text{Bi}_{0.5}\text{Na}_{0.5})\text{TiO}_3 - x\text{SrTiO}_3$ ceramics that d_{33} increases linearly with d_w . The distorted lattices of KNN under compressive stresses may also account for the shift of T_C in SPT and SPS KNN ceramics.

4. Conclusion

We conclude that d_{33} (108 pC N⁻¹), g_{33} (21.2×10⁻³ Vm N⁻¹), P_r (19.7 μC cm⁻²) and E_c (11.9 kV cm⁻¹) are significantly improved in undoped KNN ceramics processed by Spark Plasma Texturing, SPT. We also conclude that SPT KNN ceramics have a more homogeneous electrical microstructure. SPT allows fabrication at low temperatures (1000 °C) for short period (20 min) to achieve dense KNN ceramics with small grain size and narrow grain size distribution. SPT, as with hot-forging, results in neck destruction, particle rearrangement, and destruction of agglomerates improving the density and limiting grain coarsening. Concomitantly this dynamic particle rearrangement during the sintering step together with a small grain size also affects point defects creation / distribution within KNN, giving rise to a rather homogeneous defect distribution. Consequently, grain cores and shells have similar resistance and capacitance behaviours, in the case of SPT KNN ceramics. We hypothesise here that, the electrical homogeneity of SPT KNN ceramics may along with the smaller grain size and higher density increase electric breakdown strength (E_{BDS}) (of high relevance for industrial applications). In addition, the resultant compressively stressed lattice enhances the dielectric and piezoelectric performance.

We have described the interplay between materials structure, microstructure, electrical conductivity, and non-linear dielectric properties for SPT KNN and the implications of these relations for enhancing electrical properties. Based on our results we propose Spark Plasma Texturing (SPT), a modified spark plasma sintering (SPS) technique, in which uniaxial pressure is applied in an edge-free configuration, allowing ceramics to deform in the radial direction, as a strategy to enhance the electro-mechanical properties of lead-free potassium sodium niobate ceramics (KNN). Our work brings practical understanding to sintering of KNN ceramics and highlights alternative strategies for improved lead-free piezoelectrics. We envisage that the methodology may be used to optimise the performance of doped KNN as well as other Pb-free systems.

Acknowledgements

This work was developed within the scope of the project CICECO-Aveiro Institute of Materials (FCT Ref. UID/CTM/50011/2019), financed by national funds through the FCT/MCTES. The authors acknowledge the critical analysis of the impedance spectroscopy data and constructive input of Professor Derek Sinclair (University of

Sheffield). Rui Pinho acknowledges FCT for financial support, under the scholarship SFRH/BD/120969/2016. Ian M. Reaney acknowledges the support of Engineering and Physical Sciences Council research grant, EP/L017563/1.

Data Availability

Supplementary data associated with this article can be found, in the on line version, at XXX.

Conflict of Interests

The authors declare no conflict of interests.

References

- [1] Markets and Markets, “Piezoelectric Devices Market by Material, Product, Application - Global Forecast to 2022 MarketsandMarkets”.
- [2] J. Rödel, W. Jo, K.T.P. Seifert, E.-M. Anton, T. Granzow, D. Damjanovic, Perspective on the Development of Lead-free Piezoceramics, *J. Am. Ceram. Soc.*, 92 6 (2009) pp. 1153–1177, DOI: 10.1111/j.1551-2916.2009.03061.x
- [3] European Commission, “Directive 2011/65/EU of the European Parliament and of the council of 8 June 2011 - ROHS”, *Off. J. Eur. Union*, 54, 1 July (2011) pp. 88–110.
- [4] Y. Saito, H. Takao, T. Tani, T. Nonoyama, K. Takatori, T. Homma, T. Nagaya, M. Nakamura, Lead-free piezoceramics, *Nature* 432, (2004) pp. 84–87, DOI: 10.1038/nature03028
- [5] J. Rödel, K.G. Webber, R. Dittmer, W. Jo, M. Kimura, D. Damjanovic, Transferring lead-free piezoelectric ceramics into application, *J. Eur. Ceram. Soc.*, 35, 6 (2015) pp. 1659–1681, DOI: 10.1016/j.jeurceramsoc.2014.12.013
- [6] T. Ibn-Mohammed, S.C.L. Koh, I.M. Reaney, A. Acquaye, D. Wang, S. Taylor, A. Genovese, Integrated hybrid life cycle assessment and supply chain environmental profile evaluations of lead-based (lead zirconate titanate): Versus lead-free (potassium sodium niobate) piezoelectric ceramics, *Energy Environ. Sci.*, 9 11 (2016) pp. 3495–3520. DOI: 10.1039/c6ee02429g
- [7] J. Wu, D. Xiao, J. Zhu, Potassium-sodium niobate lead-free piezoelectric materials: Past, present, and future of phase boundaries, *Chem. Rev.*, 115, 7 (2015) pp. 2559–2595, DOI: 10.1021/cr5006809

- [8] C-H. Hong, H.-P. Kim, B.-Y. Choi, H-S. Han, J.S. Son, C.W. Ahn, W. Jo, Lead-free piezoceramics – Where to move on?, *J. Materiomics*, 2, 1 (2016) pp. 1–24. DOI: 10.1016/j.jmat.2015.12.002
- [9] H. Birol, D. Damjanovic, N. Setter, Preparation and characterization of $(K_{0.5}Na_{0.5})NbO_3$ ceramics, *J. Eur. Ceram. Soc.*, 26, 6 (2006) pp. 861–866. DOI: 10.1016/j.jeurceramsoc.2004.11.022
- [10] T. Hungria, J. Galy, A. Castro, Spark plasma sintering as a useful technique to the nanostructuring of piezo-ferroelectric materials, *Adv. Eng. Mater.*, 11, 8 (2009) pp. 615–631. DOI: 10.1002/adem.200900052
- [11] Z.A. Munir, U. Anselmi-Tamburini, M. Ohyanagi, The effect of electric field and pressure on the synthesis and consolidation of materials: A review of the spark plasma sintering method”, *J. Mater. Sci.*, 41, 3 (2006) pp. 763–777. DOI: 10.1007/s10853-006-6555-2
- [12] R.E. Jaeger, L. Egerton, Hot Pressing of Potassium-Sodium Niobates, *J. Am. Ceram. Soc.*, 45, 5 (1962) pp. 209–213,. DOI: 10.1111/j.1151-2916.1962.tb11127.x
- [13] G.H. Haertling, Properties of Hot-Pressed Ferroelectric Alkali Niobate Ceramics, *J. Am. Ceram. Soc.*, 50, 6 (1967) pp. 329–330. DOI: 10.1111/j.1151-2916.1967.tb15121.x
- [14] J.G. Fisher, A. Bencan, M. Kosec, S. Vernay, D. Rytz, Growth of dense single crystals of potassium sodium niobate by a combination of solid-state crystal growth and hot pressing, *J. Am. Ceram. Soc.*, 91, 5 (2008) pp. 1503–1507. DOI: 10.1111/j.1551-2916.2008.02324.x
- [15] K.L. Li, F.L. Li, Y. Wang, K.W. Kwok, H.L.W. Chan, Hot-pressed $K_{0.48}Na_{0.52}Nb_{1-x}Bi_xO_3$ ($x = 0.05-0.15$) lead-free ceramics for electro-optic applications, *Mater. Chem. Phys.*, 131, 1–2 (2011), pp. 320–324. DOI: 10.1016/j.matchemphys.2011.09.048
- [16] M. Bah, F. Giovannelli, F. Schoenstein, G. Feuillard, E. Le Clezio, I. Monot-Laffez, Synthesis, microstructure and electromechanical properties of undoped $(K_{0.5}Na_{0.5})NbO_3$, *Adv. Appl. Ceram.*, 114, 4 (2015) pp. 211–219. DOI: 10.1179/1743676114Y.0000000230
- [17] J.A. Eiras, R.B.Z. Gerbasi, J.M. Rosso, D.M. Silva, L.F. Cotica, I.A. Santos, C.A. Souza, M.H. Lente, Compositional design of dielectric, ferroelectric and piezoelectric properties of $(K,Na)NbO_3$ and $(Ba, Na)(Ti,Nb)O_3$ based ceramics

- prepared by different sintering routes, *Materials*, 9, 3 (2016) pp. 1–12. DOI: 10.3390/ma9030179
- [18] J.-F. Li, K. Wang, B.-P. Zhang, L.-M. Zhang, Ferroelectric and piezoelectric properties of fine-grained $\text{Na}_{0.5}\text{K}_{0.5}\text{NbO}_3$ lead-free piezoelectric ceramics prepared by spark plasma sintering, *J. Am. Ceram. Soc.*, 89, 2 (2006) pp. 706–709. DOI: 10.1111/j.1551-2916.2005.00743.x
- [19] M.A. Rafiq, M.E. Costa, P.M. Vilarinho, Establishing the domain structure of $(\text{K}_{0.5}\text{Na}_{0.5})\text{NbO}_3$ (KNN) single crystals by piezoforce-response microscopy, *Sci. Adv. Mater.*, 6, 3 (2014) pp. 426–433. DOI: 10.1166/sam.2014.1734
- [20] T.-L. Men, F.-Z. Yao, Z.-X. Zhu, K. Wang, J.-F. Li, Piezoelectric properties of $(\text{K}_{0.5}\text{Na}_{0.5})\text{NbO}_3$ - BaTiO_3 lead-free ceramics prepared by spark plasma sintering, *J. Adv. Dielectr.*, 06, 02 (2016) p. 1650013. DOI: 10.1142/S2010135X16500132
- [21] O. Guillon, J.G. Julian, B. Dargatz, T. Kessel, G. Schierning, J. Räthel, M. Herrmann, Field-assisted sintering technology/spark plasma sintering: Mechanisms, materials, and technology developments, *Adv. Eng. Mater.*, 16, 7 (2014) pp. 830–849. DOI: 10.1002/adem.201300409
- [22] J.G. Noudem, D. Kenfaui, D. Chateigner, M. Gomina, Toward the enhancement of thermoelectric properties of lamellar $\text{Ca}_3\text{Co}_4\text{O}_9$ by edge-free spark plasma texturing, *Scr. Mater.*, 66, 5 (2012) pp. 258–260. DOI: 10.1016/j.scriptamat.2011.11.004
- [23] M. Bah, F. Giovannelli, F. Schoenstein, G. Feuillard, E. Le Clezio, I. Monot-Laffez, High electromechanical performance with spark plasma sintering of undoped $\text{K}_{0.5}\text{Na}_{0.5}\text{NbO}_3$ ceramics, *Ceram. Int.*, 40, 5 (2014) pp. 7473–7480. DOI: 10.1016/j.ceramint.2013.12.097
- [24] J.G. Noudem, A new process for lamellar texturing of thermoelectric $\text{Ca}_3\text{Co}_4\text{O}_9$ oxides by spark plasma sintering, *J. Eur. Ceram. Soc.*, 29, 12 (2009) pp. 2659–2663. DOI: 10.1016/j.jeurceramsoc.2009.02.002
- [25] N.B. Selvaraj, M. Fernandes, I.M. Reaney, J.C.C. Abrantes, T. Denneulin, E. Snoeck, P.M. Vilarinho, A.M. Senos, Linking sintering stresses to nano modification in the microstructure of $\text{BaLa}_4\text{Ti}_4\text{O}_{15}$ by transmission electron microscopy, *Mater. Charact.*, 142 (2018) pp. 1–8. DOI: 10.1016/j.matchar.2018.04.054
- [26] A. Tkach et al., Stain Effect on the Properties of Polar Dielectric Thin Films, In: Pogrebnjak A., Novosad V. (eds.) *Advances in Thin Films, Nanostructured*

- Materials, and Coatings. Lecture Notes in Mechanical Engineering. Springer, Singapore (2019). DOI: 10.1007/978-981-13-6133-3_32
- [27] L. Egerton, D.M. Dillon, Piezoelectric and dielectric properties of Ceramics in the System Potassium-Sodium Niobate, *J. Am. Ceram. Soc.*, 42 (1959) pp. 438–442. DOI: 10.1111/j.1151-2916.1959.tb12971.x
- [28] Y.L. Wang, D. Damjanovic, N. Klein, N. Setter, High-temperature instability of Li- and Ta-modified (K,Na)NbO₃ piezoceramics, *J. Am. Ceram. Soc.*, 91, 6 (2008) pp. 1962–1970. DOI: 10.1111/j.1551-2916.2008.02392.x
- [29] R. Wang, R. Xie, T. Sekiya, Y. Shimojo, Fabrication and characterization of potassium–sodium niobate piezoelectric ceramics by spark-plasma-sintering method, *Mat. Res. Bull.*, 39, 11 (2004) pp. 1709-1715. DOI: 10.1016/j.materresbull.2004.05.007
- [30] F. Hussain, I. Sterianou, A. Khesro, D.C. Sinclair, I.M. Reaney, p-Type/n-type behaviour and functional properties of K_xNa_(1-x)NbO₃ (0.49 < x < 0.51) sintered in air and N₂, *J. Eur. Ceram. Soc.*, 38, 9 (2018) pp. 3118-3126. DOI: 10.1016/j.jeurceramsoc.2018.03.013
- [31] M.A. Rafiq, M. Rasheed, Q.K. Muhammad, M. Waqar, M. Zubair, Structural and high temperature conduction studies of (Na_{0.46}Bi_{0.46}Ba_{0.08})(Mn_xTi_{1-x}O₃)–CuO lead-free piezoelectric ceramics, *J. Mater. Sci. Mater. Electron.*, 28, 20 (2017) pp. 15009–15020. DOI: 10.1007/s10854-017-7375-7
- [32] J.T.S. Irvine, D.C. Sinclair, A.R. West Electroceramics: Characterization by Impedance Spectroscopy, *Adv. Mater.*, 2, 3 (1990) pp. 132–138. DOI: 10.1002/adma.19900020304
- [33] M.A. Rafiq, M.E. Costa, A. Tkach, P.M. Vilarinho, Impedance analysis and conduction mechanisms of lead free potassium sodium niobate (KNN) single crystals and polycrystals: A comparison study, *Cryst. Growth Des.*, 15, 3 (2015) pp. 1289–1294. DOI: 10.1021/cg5016884
- [34] S.-J. L. Kang, Sintering Densification, Grain Growth and Microstructure, *Elsevier Butterworth-Heinemann Linacre House*, no. ISBN 978-0-7506-6385-4. (2005) pp. 9–18.
- [35] K. Lu, Sintering of nanoceramics, *Int. Mater. Rev.*, 53, 1 (2008) pp. 21–38. DOI: 10.1179/174328008X254358
- [36] S. Kim, H. Choi, S. Han, J.S. Park, M.H. Lee, T.K. Song, M-H. Kim, D. Do, W-J. Kim, A correlation between piezoelectric response and crystallographic

structural parameter observed in lead-free $(1-x)(\text{Bi}_{0.5}\text{Na}_{0.5})\text{TiO}_3-x\text{SrTiO}_3$ piezoelectrics, *J. Eur. Ceram. Soc.*, 37, 4 (2017) pp. 1379–1386. DOI: 10.1016/j.jeurceramsoc.2016.11.023

Supplementary information

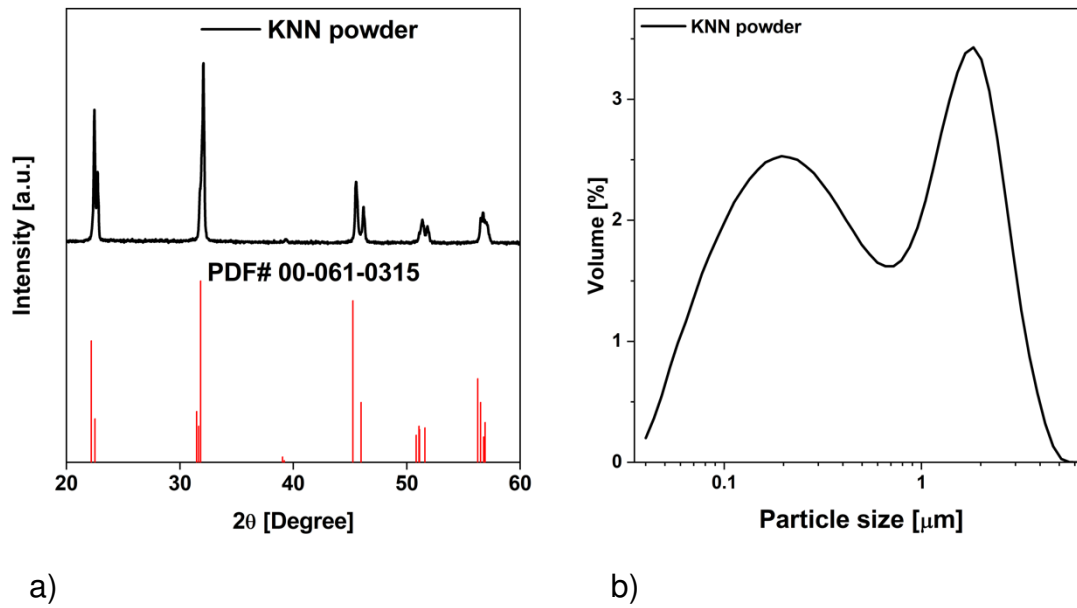
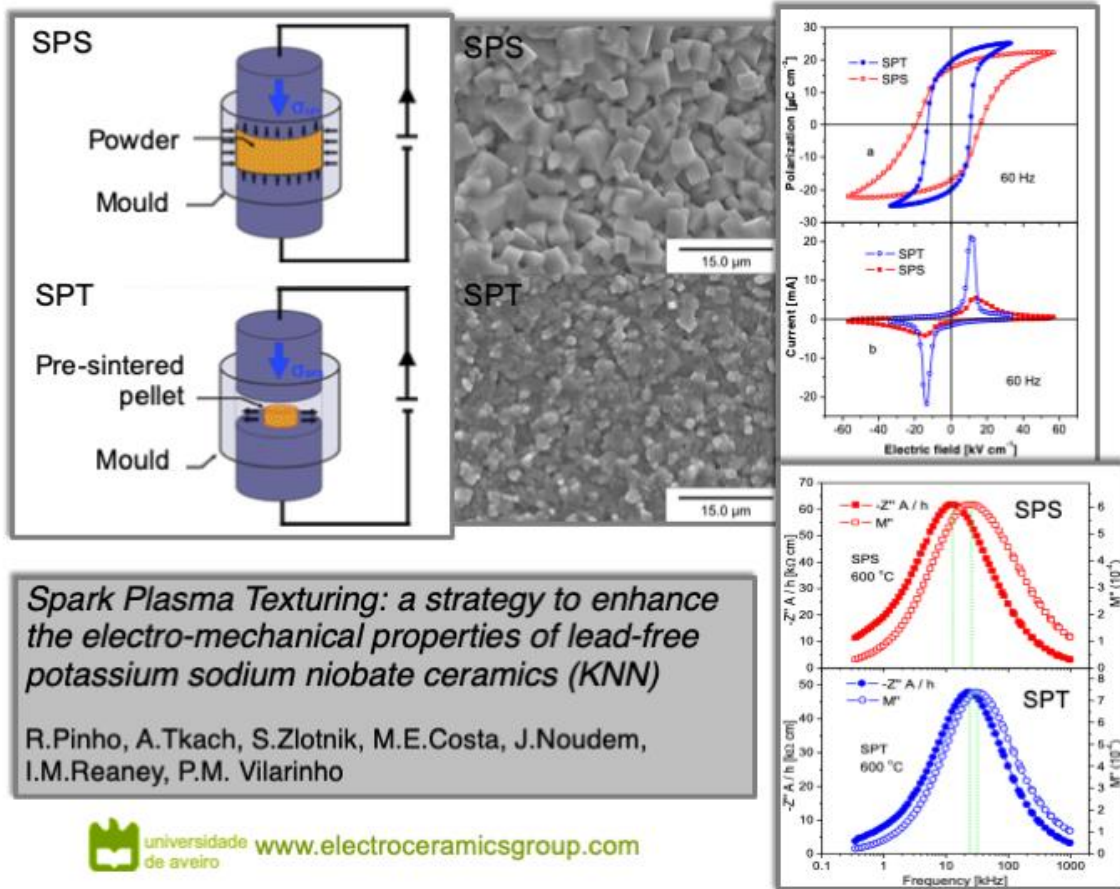


Figure S1. X-ray pattern (left, a)) and particle size distribution (right, b)) of KNN powders used to prepare SPS and SPT ceramics. The particle size distribution is bimodal with the centres at 0.2 μm and 1.8 μm.

Graphical Abstract



Spark Plasma Texturing: a strategy to enhance the electro-mechanical properties of lead-free potassium sodium niobate ceramics (KNN)

R.Pinho, A.Tkach, S.Zlotnik, M.E.Costa, J.Noudem, I.M.Reaney, P.M. Vilarinho